PHYSICAL REVIEW B VOLUME 18, NUMBER 11 1 DECEMBER 1978

Continuum-model planar channeling and the tangent-squared potential

J. A. Ellison*
Department of Physics, State University of New York at Albany, Albany, New York 12222
(Received 13 December 1977)

The elements of continuum-model planar channeling are discussed using a general planar continuum potential with an emphasis on the depth-dependent phase-space density. This joint spatial-momentum density contains all the information concerning continuum-model planar channeled particles and allows a unified treatment of the depth-dependent and statistical equilibrium, spatial, and momentum densities for an arbitrary initial density. The Gaussian-beam-divergence case is discussed in some detail. A simple, two-parameter planar-continuum potential, the tangent-squared potential, is then introduced. We show that this potential is physically reasonable, and, for many calculations, easier to use than previously used planar continuum potentials such as the Lindhard, Moliere, and hyperbolic cosine. It simplifies many calculations because the channeled-particle wavelength function and the solutions of the associated equation of motion can be written in terms of elementary functions (specifically the square root, inverse sine, and trigonometric functions) and because the phase-space density has a simple analytic form.

I. INTRODUCTION

Particle-channeling effects in crystalline materials have been pursued.[1] A complete understanding of the process requires an understanding of how the phase-space density of the channeled particles evolves as the particles move through the crystal. However, a thorough understanding is difficult since the phase space is six dimensional, the crystal atoms vibrate making the lattice look irregular to the channeled particles and the channeled particles interact with the crystal electrons in a complicated way.

In the planar-channeling case (and similarly for the axial case), it was found that an ion's motion can be reasonably approximated by using Newtonian mechanics, ignoring thermal vibration of the lattice atoms and electron multiple scattering, and replacing the atomic planes by continuum planes. A consequence of these approximations is that the velocity component of an ion parallel to the planar-channeling direction is conserved and the motion transverse to the plane is governed by a one-degree-of-freedom nonlinear oscillator. This approximation, called the planar-continuum model, represents a great simplification over the six-dimensional model with thermal vibration and multiple scattering. While it is easy to solve the nonlinear-oscillator equation numerically, there are no solutions in terms of elementary functions for the two most commonly used planar-continuum potentials of Lindhard and Moliere. An approximate planar potential, the hyperbolic cosine, which leads to solutions in terms of Jacobi elliptic functions, has been used.[2] However, in certain situations such as calculations of the depth-dependent spatial or momentum densities, this does not lead to a significant simplification.

All the information concerning the motion of continuum-model planar-channeled particles is contained in the two-dimensional, depth-dependent, phase-space density associated with the nonlinear oscillator. This density plays a fundamental role in planar channeling because (i) it is a good approximation to the actual density for depths small enough so that thermal vibrations and multiple scattering can be ignored; (ii) it has a simple representation in terms of an arbitrary initial density and the solutions of the nonlinear oscillator equation [see Eq. (2.26)]; (iii) it gives a unified framework for discussing the one-dimensional statistical equilibrium or depth-dependent, spatial, or momentum densities for any initial density, since each of these can be derived from the phase-space density by integration; (iv) it clarifies the meaning of the spatial and momentum densities for an arbitrary initial density and, in some cases, leads to simplified representations of these densities; (v) its evolution is governed by a differential equation, the Liouville equation of statistical mechanics, whereas, in contrast, the evolution of the one-dimensional spatial and momentum densities is not known to be so governed; and (vi) it forms a basis upon which departures from the simple continuum model can be discussed. These latter effects include thermal vibrations, electron multiple scattering, and discreteness of the atomic planes. We expect that a complete treatment of these effects will, of necessity, involve the phase-space density.

For channeling applications, it is not the phase-space density that needs to be determined. Backscattering experiments are sensitive to the spatial density and transmission experiments are sensitive to the momentum density, and it is these one-dimensional densities which need to be computed.

Even with the continuum model and the simple representation for the phase-space density, these one-dimensional densities are not easy to calculate.[3,4] Part of the difficulty is because the nonlinear oscillator does not generally have solutions in terms of elementary functions.

In the present work, we discuss the elements of continuum-model planar-channeling with an emphasis on the depth-dependent and statistic equilibrium phase-space densities for an arbitrary initial density. The special cases of a Gaussian and a zero beam divergence are discussed in some detail. A simple new planar-continuum potential, the tangent-squared potential, is introduced and some applications making use of it are discussed. It is our purpose to show that the tangent-squared potential is both physically reasonable and, for many applications, easier to use than previously used potentials. It is a homework exercise in Landau and Lifshitz,[5] p. 27, to show that this potential gives rise to a simple expression for the period (wavelength) as a function of energy. Also, we have found that the nonlinear oscillator defined by this potential has solutions in terms of elementary functions [see Eqs. (2.7), (2.23), (2.24), (3.1), and (3.5)–(3.6) of this paper]. In particular, the solutions can be written in terms of the square root, the inverse sine, and trigonometric functions. This leads to a closed-form representation of the phase-space density and thus, to a simplification in the calculation of the spatial and momentum densities.

In Sec. II, we discuss the planar-channeling nonlinear oscillator and show that it can be defined not only by the potential, but also by the wavelength as a function of either transverse energy or amplitude. The depth-dependent and statistical equilibrium phase-space densities are then discussed along with the corresponding spatial and momentum densities. The tangent-squared potential is discussed in Sec. III in terms of the ideas presented in Sec. II. In addition, a simple procedure is given for determining the (two) parameters in this potential so that it accurately approximates either the Lindhard or the Moliere potential. In Sec. IV, we discuss some specific channeling calculations which are significantly simplified by using the tangent-squared potential and which demonstrate that this potential is physically reasonable.

II. THEORY OF CONTINUUM-MODEL PLANAR CHANNELING

A. Equations of motion

Under the continuum approximation for planar channeling, the equation of motion associated with a channeled ion oscillating between two crystal planes (see Fig. 1) is given in Ref. 1(a) p. 154, as

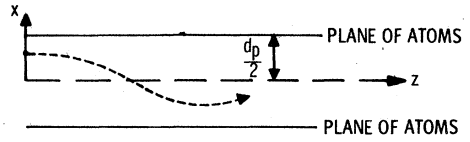

FIG. 1. Schematic for a particle undergoing channeling between two crystal planes.

$$\frac{d^2x}{dz^2}+\frac{1}{2E_z}\frac{\partial V(x)}{\partial x}=0\,, \tag{2.1}$$

where

$$V(x)=V_1(\tfrac{1}{2}d_p+x)+V_1(\tfrac{1}{2}d_p-x)-2V_1(\tfrac{1}{2}d_p)\,, \tag{2.2}$$

and $V_1(\xi)$ is the planar-continuum potential at a distance ξ from the plane, x is the transverse distance from the center of the channel, z is the distance down the channel, d_p is the interplanar spacing, and E_z is the ion's longitudinal energy (defined by the momentum component in the z direction) which, for channeling, is approximately the incident ion energy E.

The two most commonly used planar-continuum potentials are based on the Lindhard and the Moliere approximations to the Thomas-Fermi potential[1]; for the Lindhard potential,

$$\begin{aligned}V(x)&=K\{[(1+X)^2+12D^{-2}]^{1/2}\\&\quad+[(1-X)^2+12D^{-2}]^{1/2}-2(1+12D^{-2})^{1/2}\}\\&=KW_L(X,D)\end{aligned} \tag{2.3}$$

and for the Moliere potential,

$$\begin{aligned}V(x)&=K\left(\frac{0.2}{3D}e^{-(3D)}[\cosh(3XD)-1]\right.\\&\quad+\frac{1.1}{0.6D}e^{-(0.6D)}[\cosh(0.6XD)-1]\\&\quad\left.+\frac{0.7}{0.15D}e^{-(0.15D)}[\cosh(0.15XD)-1]\right)\\&=KW_M(X,D)\,,\end{aligned} \tag{2.4}$$

where X, D, and K are defined as

$$X=2x/d_p,\quad D=d_p/a_T,\quad K=\pi Z_1Z_2e^2(Nd_p)d_p\,. \tag{2.5}$$

Here a_T is the Thomas-Fermi screening radius, Z_1 and Z_2 are the atomic numbers of the projectile and target, respectively, e is the electronic charge and Nd_p is the number of atoms per unit area in the plane. For convenience the minimum value of V has been chosen as $V(0)=0$. Notice that the normalized potentials W depend only on the normalized position X and on the normalized interplanar

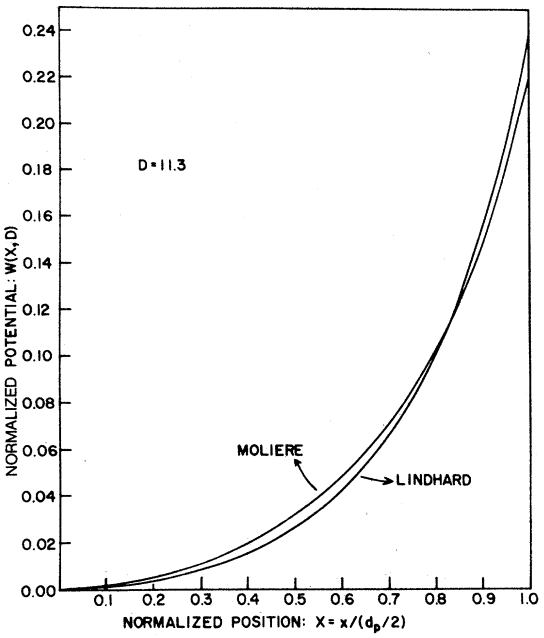

FIG. 2. Comparison of the normalized Lindhard and Moliere potentials for He incident near the {110} planes of Si.

spacing D. For the case of He incident near the (110) planes of silicon, $a_T = 0.17$ Å, $d_p = 1.92$ Å, and $D = 11.3$. The normalized Moliere and Lindhard potentials for this D value are shown in Fig. 2.

If we use Eq. (2.5) and let $Z = z/(\frac{1}{2}d_p)$ and $\epsilon = (K/E)^{1/2}$, then the equation of motion, Eq. (2.1), becomes

$$\frac{d^2X}{dZ^2} + \frac{1}{2}\epsilon^2 \frac{\partial W(X,D)}{\partial X} = 0. \tag{2.6}$$

Since D is simply a scaling parameter in W, it will be suppressed in the following: Eq. (2.6) can be written as the first-order system

$$\frac{dX}{dZ} = \epsilon\Psi \equiv \mathcal{V}_X\,, \tag{2.7a}$$

$$\frac{d\Psi}{dZ} = -\tfrac{1}{2}\epsilon W'(X) \equiv \mathcal{V}_\Psi\,, \tag{2.7b}$$

where the prime denotes differentiation of a function of one variable and Eq. (2.7a) can be viewed as the definition of Ψ. If ψ denotes the angle a trajectory makes with the planes, then $\tan\psi(Z) = dx/dz = dX/dZ$; for channeling, $\tan\psi \approx \psi$, hence

$$\Psi \approx \psi/\epsilon\,. \tag{2.8}$$

This must of course be consistent with Eq. (2.7) and the value of ϵ, that is, the initial conditions for X and Ψ and ϵ must be such that $\tan\epsilon\Psi(Z) \approx \epsilon\Psi(Z)$.

B. Properties of the nonlinear oscillator in Eq. (2.7)

Equation (2.7) is the equation of motion of a nonlinear oscillator and has an associated conservation law

$$\Psi^2 + W(X) = e_\perp = E_\perp/K\,, \tag{2.9}$$

where $e_\perp$ is a normalized transverse energy, $E_\perp$ is the transverse energy, and K is defined in Eq. (2.5). For each $e_\perp$, Eq. (2.9) defines a curve in the phase plane. Each of these curves is called an integral curve, and the set of all these curves is the phase-plane portrait for Eq. (2.7). A typical phase-plane portrait, for symmetric potentials like Eqs. (2.3) and (2.4), is shown by the concentric ovals in Fig. 3. Notice that our normalization has placed the atomic planes at $X = \pm 1$. Because of the symmetry of the potential, each integral curve has a uniquely associated amplitude A, defined implicitly by Eq. (2.9) with $\Psi = 0$,

$$W(A) = e_\perp\,. \tag{2.10}$$

The solutions of Eq. (2.7) are periodic with wavelength Λ, depending on which integral curve the motion takes place. The wavelength as a function of amplitude can be written

$$\Lambda = (4/\epsilon)Q(A) = \lambda/(\tfrac{1}{2}d_p)\,, \tag{2.11}$$

where we have

$$\begin{aligned} Q(A) &= \int_0^A [W(A) - W(\xi)]^{-1/2}\, d\xi\,, \quad A \neq 0, \\ &= \pi[2\,W''(0)]^{-1/2}, \quad A = 0, \end{aligned} \tag{2.12}$$

and λ is the wavelength in absolute units. To conveniently write the wavelength as a function of $e_\perp$ we need the inverse $H(Y)$ of $W(X)$ for $X > 0$, defined by

$$H(W(X)) = X, \quad X \geq 0. \tag{2.13}$$

If W behaves like X^2 for small X, which is the case for W_L and W_M, then H has a square-root singularity at zero. The derivative of H is defined by

$$H'(W(X)) = 1/W'(X), \quad X > 0. \tag{2.14}$$

The amplitude A as a function of $e_\perp$ can now be written $A = H(e_\perp)$; hence, the wavelength as a function of $e_\perp$ is

$$\Lambda = (4/\epsilon)\,T(e_\perp)\,, \tag{2.15}$$

where $T(e_\perp) = Q(H(e_\perp))$. That is, from Eq. (2.12)

$$\begin{aligned} T(e_\perp) &= \int_0^{H(e_\perp)} [e_\perp - W(\xi)]^{-1/2}\, d\xi\,, \quad e_\perp \neq 0, \\ &= \pi[2W''(0)]^{-1/2}, \quad e_\perp = 0. \end{aligned} \tag{2.16}$$

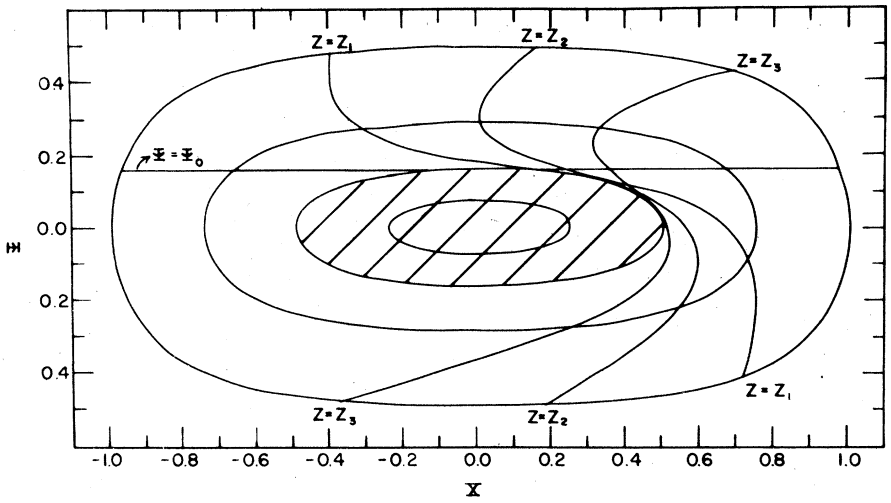

FIG. 3. Phase flow in the phase plane for various depths for particles starting along the line $\Psi = \Psi_0$ with X such that $\Psi_0^2 + W(X) \leq W(1)$. The particles never enter the shaded region, hence the density is always zero there.

We remind the reader that the functions Q, H, and T also depend on the parameter D, which has been suppressed in the notation. Notice that each phase-space point (X, Ψ) has an associated wavelength given by

$$\Lambda(X,\Psi) = (4/\epsilon)Q(H(\Psi^2 + W(X))) = (4/\epsilon)T(\Psi^2 + W(X)). \tag{2.17}$$

The primary qualitative feature of the nonlinear oscillator for planar channeling is that the wavelength is a monotonically decreasing function of amplitude with zero slope at zero amplitude (sometimes called a hard-spring oscillator). This is illustrated in Fig. 4 where we have plotted the results of numerically computing $Q(A, D)$ in Eq. (2.12) as a function of A for various D using the Moliere potential. This figure is taken from Ref. 6; a similar figure results if the Lindhard potential is used. Using Eq. (2.11) and interpolation in Fig. 4, the wavelength in absolute units as a function of amplitude can be determined for an arbitrary case. Notice that Q is qualitatively similar to the cosine function. We pursue some quantitative ramifications of this in Sec. III after showing that the tangent-squared potential gives rise to a cosine function for Q.

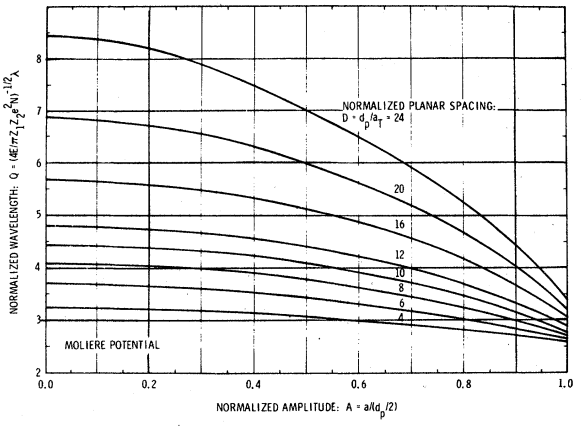

FIG. 4. Universal curves of normalized wavelength Q vs normalized amplitude A for planar-channeled particles as a function of the normalized planar spacing $D = d_p/a_T$. These calculated curves are for the Moliere potential. The λ and a are the wavelength and amplitude in absolute units and the other parameters are described in Sec. IIA.

We now have four functions, $W(X)$, $H(Y)$, $Q(A)$, and $T(e_\perp)$, related to the nonlinear oscillator of Eq. (2.7). Clearly, given either W or H, the remaining three functions can be determined. It is natural to ask whether Q or T determine the other three. Since W is a symmetric potential, H is determined from T by

$$H(Y) = \frac{1}{\pi}\int_0^Y (Y-\xi)^{-1/2} T(\xi)\, d\xi\ ; \tag{2.18}$$

hence, T determines the other three functions. This equation is derived from Eq. (2.16) in Landau and Lifschitz[5], p.27ff. Gibson and Golovchenko[7] have made use of Eq. (2.18) to determine the potential from experimental data for T. Since H depends linearly on T, superposition is possible.

The analogous relation between H and Q is more complicated,

$$H(Y)=\frac{1}{\pi}\int_0^Y (Y-\xi)^{-1/2}Q(H(\xi))\,d\xi\,. \tag{2.19}$$

This follows from Eq. (2.18) by noting that $T(\xi)=Q(\boldsymbol{H}(\xi))$. Equation (2.19) is a nonlinear Volterra integral equation for the unknown $\boldsymbol{H}$, given Q. We have not found general conditions on Q to ensure that Eq. (2.19) has a solution. However, it can be shown that if Q is such that a solution exists, and if Q is differentiable, then the solution $\boldsymbol{H}$ is unique. Furthermore, under these assumptions, it can be shown that if Q_1 is close to Q_2 then the corresponding H_1 and H_2 must be close. It follows that under certain assumptions on W [perhaps $W(X)=O(X^2)$ as $X\to 0$], H, T, or Q [perhaps $Q(0)$ is finite and $Q'(0)=0$] the four functions are equivalent. However, because of the nature of Eq. (2.19), it is difficult to construct H, W, and T given Q. General conditions aside, it can be shown that the four functions generated by either the Lindhard, the Moliere, or the tangent-squared potentials are equivalent.

C. Channeled-particle depth-dependent phase-space density

All the information for the continuum-model planar-channeled particles is contained in the phase-space density $\sigma(Z,X,\Psi)$ where $\int_\Gamma \sigma\,dX\,d\Psi$ is a measure of the number of channeled particles in an area Γ of the phase plane (see Fig. 3) at a normalized distance Z down the channel. Since the number of particles leaving any area in the phase plane must equal the rate of decrease of the number of particles in the same area, the divergence theorem can be used to show that the evolution of σ is governed by

$$\frac{\partial\sigma}{\partial t}+\nabla\cdot(\sigma\vec{\upsilon})=0\,. \tag{2.20a}$$

Here, ∇ is the divergence vector $(\partial/\partial X,\partial/\partial\Psi)$ and $\vec{\upsilon}(X,\Psi)$ is the phase-plane velocity of an ion at phase point (X,Ψ) as defined by its two components υ_X and υ_Ψ of Eq. (2.7). [Note that Eq. (2.20a) is identical in form with the continuity equation of fluid mechanics.] The right-hand side of Eq. (2.7) is divergence-free, therefore $\nabla\cdot(\sigma\vec{\upsilon})=\vec{\upsilon}\cdot\nabla\sigma$ and Eq. (2.20a) can be written

$$\frac{\partial\sigma}{\partial Z}+\epsilon\Psi\frac{\partial\sigma}{\partial X}-\tfrac{1}{2}\epsilon W'(X)\frac{\partial\sigma}{\partial\Psi}=0\,. \tag{2.20b}$$

This is the Liouville equation of classical statistical mechanics (for example see Ref. 8, p.76ff).

Since the density governed by Eq. (2.20b) contains all the information for planar-channeled particles within the continuum approximation it can be viewed as the fundamental equation of continuum-model planar channeling. It is natural, therefore, to use this equation as a starting point for the introduction of thermal vibrations or electron multiple scattering. Kumakhov[9] and Kumakhov and Wedell[10] have studied multiple scattering from electrons using a Fokker-Planck equation which reduces to Eq. (2.20b) when the multiple scattering is ignored. In order to understand multiple scattering effects and distinguish them from continuum effects, it is helpful to have a good understanding of the continuum-model phase-space density.

Equation (2.20b) is a first-order partial differential equation which can be solved by the method of characteristics. The idea of this method is to look for curves (called characteristics) $X=X(Z)$, $\Psi=\Psi(Z)$ in X-Ψ-Z space on which the partial differential equation reduces to an ordinary differential equation. On an arbitrary curve, the rate of change of $\sigma(Z,X(Z),\Psi(Z))$ with respect to Z is given by

$$\frac{d\sigma}{dZ}=\frac{\partial\sigma}{\partial Z}+\frac{\partial\sigma}{\partial X}\frac{dX}{dZ}+\frac{\partial\sigma}{\partial\Psi}\frac{d\Psi}{dZ}\,. \tag{2.21}$$

If the curve is now chosen so that $X(Z)$ and $\Psi(Z)$ are solutions of Eq. (2.7) then the right-hand side of Eq. (2.21) is zero [since σ is assumed to be a solution of Eq. (2.20b)] and Eq. (2.21) reduces to the trivial ordinary differential equation $d\sigma/dZ=0$ along this curve. It follows that σ is a constant on the curves in X-Ψ-Z space determined by solutions of Eq. (2.7), that is, the density following a particle in phase space is constant. This is the standard content of the Liouville theorem in classical mechanics. If the phase-space density at $Z=0$ is denoted by $\sigma_0(X,\Psi)$, then it follows that

$$\sigma(Z,X(Z),\Psi(Z))=\sigma(0,X_i,\Psi_i)=\sigma_0(X_i,\Psi_i)\,, \tag{2.22}$$

where $X_i=X(0)$ and $\Psi_i=\Psi(0)$. The relationship between (X,Ψ) and (X_i,Ψ_i) in this equation can be conveniently written

$$\begin{pmatrix}X\\ \Psi\end{pmatrix}=\overline{\varphi}(Z,X_i,\Psi_i)\equiv\begin{pmatrix}\varphi_1(Z,X_i,\Psi_i)\\ \varphi_2(Z,X_i,\Psi_i)\end{pmatrix}, \tag{2.23}$$

where $\overline{\varphi}$ satisfies the following initial-value problem for Eq. (2.7):

$$\begin{aligned}&\frac{\partial\varphi_1}{\partial Z}=\epsilon\varphi_2,\quad \varphi_1(0,X_i,\Psi_i)=X_i\,,\\ &\frac{\partial\varphi_2}{\partial Z}=-\tfrac{1}{2}\epsilon W'(\varphi_1),\quad \varphi_2(0,X_i,\Psi_i)=\Psi_i\,.\end{aligned} \tag{2.24}$$

Equation (2.23) states that the phase point (X_i,Ψ_i) moves to the phase point (X,Ψ) in Z units. Since Eq. (2.7) does not depend explicitly on Z, the phase point (X,Ψ) must move back to (X_i,Ψ_i) in $-Z$ units. Hence, the inverse relation is

$$\begin{pmatrix}X_i\\ \Psi_i\end{pmatrix}=\overline{\varphi}(-Z,X,\Psi)\,. \tag{2.25}$$

Using Eqs. (2.22) and (2.25), the solution of the Liouville equation (2.20b) with the initial density σ_0 becomes[11]

$$\sigma(Z, X, \Psi) = \sigma_0(\varphi_1(-Z, X, \Psi), \varphi_2(-Z, X, \Psi)). \tag{2.26}$$

It is important to notice that $\overline{\varphi}(\alpha, \beta, \gamma)$ denotes the phase-space position which has evolved from phase point (β, γ) in α units. Also, the inverse relations (2.23) and (2.25) are a special case of the more general property

$$\overline{\varphi}(Z_1 + Z_2, X, \Psi) = \overline{\varphi}(Z_2, \varphi_1(Z_1, X, \Psi), \varphi_2(Z_1, X, \Psi)), \tag{2.27}$$

which follows from the fact that both sides of Eq. (2.27) satisfy the same initial value problem for Eq. (2.7) in the independent variable Z_2. Geometrically, this equation says that moving Z_1 units from phase point (X, Ψ) and then Z_2 units from the evolved phase point $(\varphi_1(Z_1, X, \Psi), \varphi_2(Z_1, X, \Psi))$ is the same as moving $Z_1 + Z_2$ units from (X, Ψ).

Equation (2.26) is our fundamental result concerning the phase-space density. It is both simple in form and contains all the information concerning planar-channeled particles for an arbitrary initial density. It represents a unification in that all depth-dependent or statistical equilibrium, spatial or momentum densities for any σ_0 can be derived from it. In comparison with previously derived representations for the spatial or momentum density, it is both more general (σ_0 is arbitrary) and simpler in form. It gives a closed-form expression for the phase-space density if the functions φ_1 and φ_2 can be determined analytically. This is the case for the tangent-squared potential to be discussed in Sec. III. To compute $\sigma(Z, X, \Psi)$ in the case where φ_1 and φ_2 cannot be determined analytically (which is the case for most planar-channeling potentials), the differential equations in Eq. (2.7) must be integrated backward, Z units from the phase point (X, Ψ). For large Z, it is convenient to take advantage of the periodicity of σ in Z, that is, $\sigma(Z + \Lambda(X, \Psi), X, \Psi) = \sigma(Z, X, \Psi)$, where $\Lambda(X, \Psi)$ is defined in Eq. (2.17). This periodicity follows from Eq. (2.26) and the periodicity of φ_1 and φ_2.

We define a particle to be channeled if its amplitude $A \leq A_c$, where A_c is a critical amplitude; hence, Eq. (2.26) holds for all X and Ψ such that $\Psi^2 + W(X) \leq W(A_c)$. Since σ represents the channeled density, $\sigma = 0$ for all X, Ψ such that $\Psi^2 + W(X) > W(A_c)$. To complete the picture, the nonchanneled particles must also be incorporated[1,4]; however, these particles will not be considered in this paper.

The results of a channeling experiment are typically sensitive to either the spatial density $\rho_X(Z, X)$ or the momentum density $\rho_\Psi(Z, \Psi)$; hence, for comparison with experiment, it is not the joint density σ, but the corresponding one-dimensional densities which need to be computed. These densities are the integral of the phase-space density σ over the Ψ interval $[-b, b]$ where $b^2 = W(A_c) - W(X)$ or over the X interval $[-b, b]$, where $b = H(W(A_c) - \Psi^2)$. This makes clear the meaning of these one-dimensional densities in the case of an arbitrary initial density σ_0.

D. Density discussion for special σ_0

In a channeling experiment, it is generally assumed that the initial spatial density is uniform and the initial momentum density is Gaussian with small variance. The latter corresponds to a small beam divergence with a Gaussian distribution. We first pursue the idealized case of zero beam divergence; hence,

$$\sigma_0(X, \Psi) = \tfrac{1}{2}\delta(\Psi - \Psi_0), \tag{2.28}$$

where δ denotes the delta function,

$$\Psi_0 = \tan(\psi_0/\epsilon) \approx \psi_0/\epsilon \equiv (E/K)^{1/2}\psi_0, \tag{2.29}$$

and ψ_0 is the incident angle in radians. The initial positions of the particles in the phase plane are shown by the horizontal line in Fig. 3 and the initial density is uniformly distributed along this line. The channeled-particle phase-space density in Eq. (2.26) becomes

$$\sigma(Z, X, \Psi) = \tfrac{1}{2}\delta(\varphi_2(-Z, X, \Psi) - \Psi_0), \quad \Psi^2 + W(X) \leq W(A_c). \tag{2.30}$$

The position of the particles at three depths, $Z_1 < Z_2 < Z_3$, are shown by the nonoval (phase flow) curves in Fig. 3. It should be noted, however, that the density is not uniform along these curves.

The spatial density, obtained by integrating Eq. (2.30) over Ψ, is given by[12]

$$\rho_X(Z, X) = \frac{1}{2}\sum_i \left| \frac{\partial \varphi_2}{\partial \Psi}(-Z, X, \Psi_i) \right|^{-1}, \tag{2.31a}$$

where the sum is over all i such that $\Psi_i(Z, X, \Psi_0)$ satisfies

$$\varphi_2(-Z, X, \Psi_i) - \Psi_0 = 0 \quad \text{and} \quad \Psi_i^2 + W(X) \leq W(A_c). \tag{2.31b}$$

Similarly, the momentum density is found to be

$$\rho_\Psi(Z, \Psi) = \frac{1}{2}\sum_i \left| \frac{\partial \varphi_2}{\partial X}(-Z, X_i, \Psi) \right|^{-1}, \tag{2.32a}$$

where the sum is over all i such that $X_i(Z, \Psi, \Psi_0)$ satisfies

$$\varphi_2(-Z, X_i, \Psi) - \Psi_0 = 0 \quad \text{and} \quad \Psi^2 + W(X_i) \leq W(A_c) . \tag{2.32b}$$

Equivalent representations for the spatial and momentum densities can be derived geometrically using the phase plane as discussed in Ref. 4. Briefly, the argument for the momentum density is that

$$\rho_\Psi(Z, \Psi)\Delta\Psi \simeq \frac{1}{2} \sum_{i=1}^{N} \Delta X_{0i} , \tag{2.33}$$

where ΔX_{0i} is the ith initial spatial interval which gets mapped into the interval $\Delta\Psi$ at normalized depth Z. The N intervals $\{\Delta X_{0i}\}$ are neighborhoods of the initial points X_{0i} satisfying $\varphi_2(Z, X_{0i}, \Psi_0) - \Psi = 0$. Therefore,

$$\rho_\Psi(Z, \Psi) = \frac{1}{2} \sum_i \left| \frac{\partial \varphi_2}{\partial X}(Z, X_{0i}, \Psi_0) \right|^{-1} , \tag{2.34a}$$

where the sum is over all i such that X_{0i} satisfies

$$\varphi_2(Z, X_{0i}, \Psi_0) - \Psi = 0 \quad \text{and} \quad \Psi_0^2 + W(X_{0i}) \leq W(A_c) . \tag{2.34b}$$

Similarly, the spatial density is given by

$$\rho_X(Z, X) = \frac{1}{2} \sum_i \left| \frac{\partial \varphi_1}{\partial X}(Z, \tilde{X}_{0i}, \Psi_0) \right|^{-1} , \tag{2.35a}$$

where the sum is over all i such that $\tilde{X}_{0i}$ satisfies

$$\varphi_1(Z, \tilde{X}_{0i}, \Psi_0) - X = 0 \quad \text{and} \quad \Psi_0^2 + W(\tilde{X}_{0i}) \leq W(A_c) . \tag{2.35b}$$

The representations of Eqs. (2.34) and (2.35) appear to be a simplification of Eqs. (2.31) and (2.32), since the latter requires knowledge of $\overline{\varphi}(-Z, X, \Psi)$ for all X and Ψ whereas the former requires knowledge of $\overline{\varphi}(Z, X, \Psi_0)$ for all X but Ψ_0 fixed. The depth-dependent spatial density ρ_X has been computed by Abel *et al.*[3] using Eq. (2.35) with a simple approximation to φ_1 and $\Psi_0 = 0.0$ and by Ellison[4] using Eq. (2.35) with $\partial\varphi_1/\partial X$ determined by numerically computing the solution of Eq. (2.7) and the associated variational equation.

The equivalence of the corresponding representations can be derived by differentiating Eq. (2.23) with respect to X and Ψ (with X_i and Ψ_i as in Eq. (2.25)), making use of the fact that the Jacobian of the transformation $\overline{\varphi}(Z, -, -)$ is 1, that is

$$\begin{vmatrix} \frac{\partial \varphi_1}{\partial X} & \frac{\partial \varphi_1}{\partial \Psi} \\ \frac{\partial \varphi_2}{\partial X} & \frac{\partial \varphi_2}{\partial \Psi} \end{vmatrix} = 1 , \tag{2.36}$$

and noting that the Ψ_i and $\tilde{X}_{0i}$ can be chosen so that

$$\overline{\varphi}(Z, \tilde{X}_{0i}, \Psi_0) = \begin{pmatrix} X \\ \Psi_i \end{pmatrix} \quad \text{or} \quad \overline{\varphi}(-Z, X, \Psi_i) = \begin{pmatrix} \tilde{X}_{0i} \\ \Psi_0 \end{pmatrix} \tag{2.37a}$$

and that the X_i and X_{0i} can be chosen so that

$$\overline{\varphi}(Z, X_{0i}, \Psi_0) = \begin{pmatrix} X_i \\ \Psi \end{pmatrix} \quad \text{or} \quad \overline{\varphi}(-Z, X_{0i}, \Psi) = \begin{pmatrix} X_{0i} \\ \Psi_0 \end{pmatrix} . \tag{2.37b}$$

In the more general case of a Gaussian beam divergence, the initial density is given by

$$\sigma_0(X, \Psi) = \tfrac{1}{2} g(\Psi - \Psi_0) , \tag{2.38}$$

where g is a Gaussian density and Ψ_0 is the mean value of the initial momenta. The spatial density in this case is

$$\rho_X(Z, X; g) = \frac{1}{2} \int_{-b}^{b} g(\varphi_2(-Z, X, \Psi) - \Psi_0)\, d\Psi , \tag{2.39}$$

where $b^2 = W(A_c) - W(X)$. The integrand can be written $\int g(\xi - \Psi_0)\delta(\varphi_2(-Z, X, \Psi) - \xi)\, d\xi$; hence, another representation of this density is

$$\rho_X(Z, X; g) = \int g(\xi - \Psi_0) \times \left(\frac{1}{2} \int_{-b}^{b} \delta(\varphi_2(-Z, X, \Psi) - \xi)\, d\Psi \right) d\xi . \tag{2.40}$$

This representation is not surprising since the term in brackets is just the spatial density for the case of zero beam divergence as given in either Eq. (2.31) or Eq. (2.35). In contrast to the zero beam divergence case, the representation of Eq. (2.39) derived directly from the phase-space density, is easier to use for computing the density than is Eq. (2.40). The momentum density is similar.

E. Densities in statistical equilibrium

Since $\sigma(Z, X, \Psi)$ is a periodic function of Z, the associated statistical equilibrium density $\bar{\sigma}$ is given by the average of σ over one period. Using Eq. (2.26),

$$\bar{\sigma}(X, \Psi) = \frac{1}{\Lambda} \int_0^{\Lambda} \sigma_0(\varphi_1(Z, X, \Psi), \varphi_2(Z, X, \Psi))\, dZ , \tag{2.41}$$

where $\Lambda(X, \Psi)$ is defined in Eq. (2.17) and we have made the change of variable from Z to $-Z$. The periodicity of $\overline{\varphi}$ and the fact that, by Eq. (2.27), there exists an $\alpha(X, \Psi)$ such that $\overline{\varphi}(Z, X, \Psi) = \overline{\varphi}(Z + \alpha, 0, e_1^{1/2})$, allow $\bar{\sigma}$ to be rewritten

$$\bar{\sigma}(X,\Psi)=f(e_\perp(X,\Psi))\equiv\frac{1}{(4/\epsilon)T(e_\perp)}\int_0^{(4/\epsilon)T(e_\perp)}\sigma_0(\varphi_1(Z,0,e_\perp^{1/2}),\varphi_2(Z,0,e_\perp^{1/2}))\,dZ\,. \tag{2.42}$$

Here $e_\perp$ and $T(e_\perp)$ are defined in Eqs. (2.9) and (2.16). This shows explicitly that the statistical-equilibrium density at phase point (X,Ψ) depends only on the transverse energy associated with that point. Equation (2.42) is a line integral around the closed-integral curve $\gamma(e_\perp)$ defined by Eq. (2.9), and can be written

$$\bar{\sigma}(X,\Psi)=\frac{1}{4T(e_\perp)}\oint_{\gamma(e_\perp)}(\{\Psi^2+\tfrac{1}{4}[W'(X)]^2\}^{-1/2}\sigma_0(X,\Psi))\,ds\,, \tag{2.43}$$

where s is the arc length along γ and is related to Z by $(ds/dZ)^2=\epsilon^2\{\Psi^2+\frac{1}{4}[W'(X)]^2\}$. The X and Ψ in the integrand denote the phase point on the integral curve γ as a function of arc length and should not be confused with arguments the X and Ψ of $\bar{\sigma}$.

Added insight into Eqs. (2.42) and (2.43) can be gained by deriving the statistical-equilibrium-phase space density in an alternate way. This derivation proceeds by introducing a new set of coordinates, determining the density in these new coordinates, and then transforming back to X and Ψ.

The phase point represented by the coordinates (X,Ψ) can be equivalently represented by the coordinates $(Z,e_\perp)$, where these are related by

$$\begin{pmatrix}X\\ \Psi\end{pmatrix}=\bar{\varphi}(Z,0,e_\perp^{1/2})\,, \tag{2.44}$$

for $0\le Z\le(4/\epsilon)T(e_\perp)$. The transverse energy $e_\perp$ fixes one of the integral curves (ovals, as shown in Fig. 3) and Z, which is the distance down the channel traveled by a particle which starts at $X=0$, $\Psi=e_\perp^{1/2}$, tags the particular phase point on the integral curve. The Jacobian $\partial(X,\Psi)/\partial(Z,e_\perp)$ of the transformation Eq. (2.44) is $\frac{1}{2}\epsilon$; hence, the densities in two-coordinate systems are related by

$$\bar{\sigma}(X,\Psi)=\bar{\sigma}_{Ze_\perp}(Z,e_\perp)(2/\epsilon)\,. \tag{2.45}$$

Let $p_c(Z/e_\perp)\Delta Z$ denote the conditional probability of a channeled ion being in the interval of distance down the channel, ΔZ, given it has transverse energy $e_\perp$. Since the particle moves down the channel at a constant velocity, this probability is given by

$$p_c(Z/e_\perp)\Delta Z=\frac{\Delta Z}{(4/\epsilon)T(e_\perp)}\,. \tag{2.46}$$

If $p_e(e_\perp)$ denotes the transverse-energy density, which does not change as the ions penetrate the crystal because of the conservation of the energy, then the joint density is given by

$$\bar{\sigma}_{Ze_\perp}(Z,e_\perp)=p_c(Z/e_\perp)p_e(e_\perp)=\frac{\epsilon}{4T(e_\perp)}p_e(e_\perp)\,. \tag{2.47}$$

Using Eq. (2.45), the density in (X,Ψ) coordinates is given by

$$\bar{\sigma}(X,\Psi)=p_e(e_\perp)/2T(e_\perp)\,, \tag{2.48}$$

and is seen to be proportional to the transverse-energy density divided by the wavelength. The transverse-energy density can be determined by noting that Eq. (2.45) also holds for the initial density σ_0; hence,

$$\begin{aligned}p_e(e_\perp)&=\int_0^{(4/\epsilon)T(e_\perp)}\sigma_{0Ze_\perp}(Z,e_\perp)\,dZ\\&=\frac{\epsilon}{2}\int_0^{(4/\epsilon)T(e_\perp)}\sigma_0(\varphi_1(Z,0,e_\perp^{1/2}),\varphi_2(Z,0,e_\perp^{1/2}))\\&\qquad\times dZ\,.\end{aligned} \tag{2.49}$$

Combining Eqs. (2.48) and (2.49) yields the density as derived in Eq. (2.42). Also, it is seen that the integrals in Eqs. (2.42) and (2.43) are proportional to the transverse-energy density.

The fact that $\bar{\sigma}$ depends only on $e_\perp$ means that all the information concerning the statistical equilibrium motion of continuum-model planar-channeled particles is contained in a function of one variable once the potential W and the initial density σ_0 have been chosen. This suggests the following simple algorithm for computing either the equilibrium, spatial, or momentum densities in the case of arbitrary σ_0: (i) Compute $f(e_\perp)$ of Eq. (2.42) for a few values of $e_\perp$ in the interval $[0,W(A_c)]$ and fit with an interpolating cubic spline. (ii) Find, for example, $\bar{\rho}_X$ by numerical evaluation of the integral $\bar{\rho}_X(X)=\int_{-b}^{b}f(e_\perp(X,\Psi))\,d\Psi$ where $b=[W(A_c)-W(X)]^{1/2}$.

The function $f(e_\perp)$ can be determined from Eq. (2.42) after φ_1 and φ_2 are found by numerically integrating the differential equations, Eq. (2.7). However, if the change of variable from Z to ξ by $\xi=\varphi_1(Z,0,e_\perp^{1/2})$ is made in the integral of Eq. (2.42) then $\varphi_2(Z,0,e_\perp^{1/2})=\pm[e_\perp-W(\xi)]^{1/2}$ and Eq. (2.42) becomes

$$f(e_\perp)=\frac{1}{4T(e_\perp)}\int_{-H(e_\perp)}^{H(e_\perp)}\frac{\sigma_0(\xi,\Psi(\xi))+\sigma_0(\xi,-\Psi(\xi))}{\Psi(\xi)}\,d\xi\,, \tag{2.50}$$

where $\Psi(\xi) = [e_\perp - W(\xi)]^{1/2}$. This integral bypasses solving the differential equations for φ_1 and φ_2 and is easy to evaluate numerically.

Of particular interest in channeling studies is the case of a Gaussian beam divergence where the σ_0 in Eq. (2.50) is replaced by Eq. (2.38). For zero beam divergence this reduces to[12]

$$\bar{\sigma} = f(e_\perp) = \begin{cases} 0 & , \quad e_\perp < \Psi_0 \text{ and } e_\perp > W(A_c) \\ [2T(e_\perp)W'(H(e_\perp - \Psi_0^2))]^{-1}, & \Psi_0^2 < e_\perp < W(A_c) \end{cases} . \tag{2.51}$$

This can be derived directly without introducing the δ function. From Fig. 3 it can be seen that the ions with transverse energy in $\Delta e_\perp$ are initially in the spatial interval $[H(e_\perp - \Psi_0^2), H(e_\perp + \Delta e_\perp - \Psi_0^2)]$ and its negative counterpart. Therefore, $p_e(e_\perp) = H'(e_\perp - \Psi_0^2)$ for $\Psi_0^2 < e_\perp < W(A_c)$ and equals zero otherwise. Equation (2.51) follows from Eqs. (2.13), (2.14), and (2.48). Notice that the transverse-energy density, and hence $\bar{\sigma}$, is zero in both the central shaded region and the region outside the oval with transverse energy $W(A_c)$, as shown in Fig. 3. Also, Eq. (2.51) and Eq. (18) of Ref. 6(b) are the same, if the identity $T(e_\perp) = Q(H(e_\perp))$ is noted.

The statistical equilibrium *spatial* density for the case of zero beam divergence, which can be obtained by integrating Eq. (2.51), has been derived[3,6(a)] by an argument which is similar to the content of Eq. (2.46) but does not use the phase-space density. (A thorough discussion of this density is contained in Ref. 6.) A nonzero beam divergence could be incorporated by convoluting this density with a Gaussian density as discussed in Sec. II D. However, the representation in Eq. (2.50) combined with the algorithm discussed prior to this equation appears to be a simpler approach.

The usefulness of the statistical equilibrium densities depends on knowledge of the conditions under which they can replace the corresponding depth-dependent densities. In Ref. 13 it is shown that for the case of zero beam divergence the integral of $\rho_X(Z, X)$ over an X interval I approaches the integral of $\bar{\rho}_X(X)$ over I, for large Z. Similar results presumably hold for other densities and general σ_0. For channeling studies, however, it is also important to know how fast statistical equilibrium is reached. Work is in progress on the rate of its approach to equilibrium and some preliminary results show that if $\rho_X(Z, X)$ is integrated over both I and depth, then the approach is very rapid.

III. TANGENT-SQUARED POTENTIAL

A. Properties

The tangent-squared potential is given by

$$W_T(X) = \beta \tan^2 \alpha X , \tag{3.1}$$

where $-1 \leq X \leq 1$, $0 < \alpha < \frac{1}{2}\pi$ and $\beta > 0$. The other three equivalent functions discussed in Sec. II B are

$$H_T(Y) = (1/\alpha) \arctan (Y/\beta)^{1/2}, \quad 0 \leq Y \leq \beta \tan^2 \alpha, \tag{3.2}$$

$$Q_T(A) = \frac{\pi}{2\alpha\beta^{1/2}} \cos \alpha A, \quad 0 \leq A \leq 1, \tag{3.3}$$

and

$$T_T(e_\perp) = (\pi/2\alpha)(\beta + e_\perp)^{-1/2}, \quad 0 \leq e_\perp \leq \beta \tan^2 \alpha. \tag{3.4}$$

The solutions of Eq. (2.24) can be written[14]

$$\varphi_{T_1}(Z, X, \Psi) = (1/\alpha) \arcsin[\gamma(X, \Psi) \sin \omega(Z, X, \Psi)], \tag{3.5a}$$

$$\varphi_{T_2}(Z, X, \Psi) = e_\perp^{1/2}(X, \Psi) \cos \omega / (1 - \gamma^2 \sin^2 \omega)^{1/2}, \tag{3.5b}$$

where

$$\Psi \geq 0, \tag{3.6a}$$

$$e_\perp(X, \Psi) = \Psi^2 + \beta \tan^2 \alpha X = \beta \tan^2 \alpha A , \tag{3.6b}$$

$$\gamma(X, \Psi) = [e_\perp/(\beta + e_\perp)]^{1/2} = \sin \alpha A , \tag{3.6c}$$

and

$$\omega(Z, X, \Psi) = \alpha(e_\perp + \beta)^{1/2} \epsilon Z + \arcsin(\sin \alpha X / \gamma) . \tag{3.6d}$$

From phase-plane symmetry it is seen that

$$\bar{\varphi}(Z + \tfrac{1}{2}\Lambda(X, \Psi), X, \Psi) = \bar{\varphi}(Z, -X, -\Psi) , \tag{3.7}$$

which can be used with Eqs. (3.5) and (3.6) to determine $\bar{\varphi}_T(Z,X,\Psi)$ for $\Psi<0$.

When $\Psi=0$, $\bar{\varphi}_T$ simplifies to

$$\varphi_{T_1}(Z,X,0)=(1/\alpha)\arcsin\{\sin\alpha X\cos[f(X)Z]\} \tag{3.8a}$$

and

$$\varphi_{T_2}(Z,X,0)=\frac{-\beta^{1/2}\tan\alpha X\sin fZ}{(1-\sin^2\alpha X\cos^2 fZ)^{1/2}}, \tag{3.8b}$$

where

$$f(X)=\epsilon\alpha\beta^{1/2}/\cos\alpha X\ . \tag{3.8c}$$

We now have a simple analytic expression for the depth-dependent phase-space density as given in Eqs. (2.26) and (3.5) which can be used to determine the spatial and momentum densities. We have not found any reasonable σ_0 which give simple analytical expressions for the associated one-dimensional densities. However, the above knowledge of φ_{T_1} and φ_{T_2} simplifies the amount of work involved in computing these densities.

For example, consider the problem of finding $\rho_X(Z,X)$ when $\sigma_0=\frac{1}{2}\delta(\Psi-\Psi_0)$. From Eq. (2.35), it is seen that the only real numerical work is to find all the $\tilde{X}_{0i}$ such that

$$\varphi_{T_1}(Z,\tilde{X}_{0i},\Psi_0)-X=0. \tag{3.9}$$

The partial derivative of φ_{T_1} with respect to X can be determined analytically from Eq. (3.5a) and the density can be determined by evaluating these derivatives at each $\tilde{X}_{0i}$.[15] An example of this will be discussed in Sec. IV. This technique is simpler than the one outlined in Ref. 4 for use with the Lindhard or Moliere potentials in which case $\bar{\varphi}(Z,X,\Psi_0)$ and its partial derivatives must be determined for a large number of X values by numerically computing the solutions of Eq. (2.7) and the associated variational equations. Also, because of the explicit form of Eq. (3.5), it is easier to increase the accuracy of the density calculation in the tangent-squared case than in the Lindhard or Moliere case. A simpler technique which yields an *approximation* to the one-dimensional densities for the tangent-squared potential and the δ-function initial condition will also be discussed in Sec. IV.

The incorporation of a Guassian beam divergence into the spatial density using Eq. (2.39) involves only a simple integration since g and φ_2 are known. This calculation is more straightforward and perhaps easier than the zero beam divergence case just discussed.

The calculation of the statistical equilibrium phase-space density is also simplified since the period function T and the inverse of the potential H needed in Eqs. (2.50) are given analytically in Eqs. (3.2) and (3.4). Also, for the δ-function initial condition, Eq. (2.51) takes the particularly simple form

$$\bar{\sigma}(X,\Psi)=\begin{cases}0, & e_\perp<\Psi_0^2\\ \dfrac{\beta^{1/2}}{2\pi}\dfrac{(\beta+e_\perp)^{1/2}}{(\beta+e_\perp-\Psi_0^2)(e_\perp-\Psi_0^2)^{1/2}}, & e_\perp>\Psi_0^2\ .\end{cases} \tag{3.10}$$

The one-dimensional statistical equilibrium spatial density for $\Psi_0=0$ can be determined from Eq. (3.10) in terms of the elliptic integral of the first kind. We suspect that the spatial density for $\Psi_0>0$ and the momentum density for arbitrary Ψ_0 can be determined in terms of elliptic integrals of the first, second, and third kinds. However, this does not appear to be very useful since it is straightforward to numerically compute the one-dimensional statistical equilibrium densities for a general potential as is demonstrated in Ref. 6.

The usefulness of the tangent-squared potential depends upon whether the α and β can be chosen so that there is good agreement between the densities computed using it and the densities computed using either the Lindhard or Moliere potentials. In Sec. IV it is shown that this is possible.

B. Comparison with the Lindhard and Moliere potentials

In Sec. II B we pointed out that Q_M (Q determined from the Moliere potential W_M) is qualitatively similar to a cosine function; this is also true for Q_L as can be seen in Fig. 5 where we have plotted Q_L and Q_M for $D=11.3$. Here we show that the

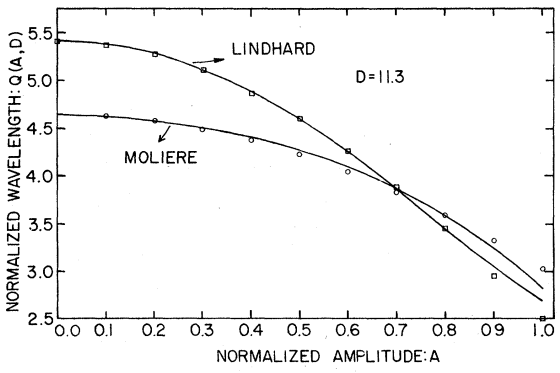

FIG. 5. Normalized wavelength Q vs normalized amplitude A for channeled particles for $D=11.3$, which corresponds to He in (110) Si. The upper curve is computed using the Lindhard potential and the lower using the Moliere potential. The open symbols are the tangent-squared approximation.

parameters, α and β, in the tangent-squared potential can be chosen so that reasonable quantitative agreement can also be obtained. We do not pursue the question of best fit since W_L and W_M are only approximate planar-continuum potentials which differ in significant ways.

Since W, H, Q, and T each equivalently determine the planar-continuum oscillator, α and β can be chosen by finding a good fit between any one of these and the corresponding function for the tangent-squared potential. Because the monotonic decrease of wavelength with amplitude (or transverse energy) is the primary qualitative feature of the planar-channeling oscillator, we favor determining α and β by fitting Q_T to Q or T_T to T. We choose to fit the Q's because of the availability of the curves in Fig. 4.

If we let

$$Q_T(A) = C\cos\alpha A\ , \tag{3.11}$$

and determine C and α by requiring that $Q_T(0) = Q(0)$ and $Q_T(A_0) = Q(A_0)$ for some $A_0 > 0$, then

$$C = Q(0) \equiv \pi/[2W''(0)]^{1/2}\ , \tag{3.12a}$$

$$\alpha = (1/A_0)\arccos[Q(A_0)/Q(0)]\ , \tag{3.12b}$$

and from Eq. (3.3)

$$\beta = (\pi/2\alpha C)^2\ . \tag{3.12c}$$

The normalized wavelength at amplitude A_0 for either the Lindhard potential $Q_L(A_0, D)$ or the Moliere potential $Q_M(A_0, D)$ is determined from Eq. (2.12) by numerical integration. However, because of the availability of the curves in Fig. 4, $Q_M(A_0, D)$ can be obtained by interpolation in the parameter D. A similar set of universal curves is easily constructed for use with the Lindhard potential.

If we choose $A_0 = 0.8$ and consider the case of 1-MeV He incident near the (110) planes of Si ($D = 11.3$), then Eq. (3.12) yields $(\alpha, \beta)_M = (0.86, 0.15)$, and $(\alpha, \beta)_L = (1.10, 0.07)$. In Fig. 5 the tangent-squared approximations to both the Lindhard and the Moliere wavelength functions are shown by the open symbols for $D = 11.3$. Similar agreement is obtained for other values of D. Note that Q_T, with α and β chosen using $Q_L(Q_M)$, is much closer to $Q_L(Q_M)$ than is $Q_M(Q_L)$. It appears, therefore, that based on current knowledge the tangent-squared potential is a satisfactory planar-continuum potential and it would be interesting to determine if this potential can be derived from a physically-reasonable screened Coulomb potential.

IV. APPLICATION

A. Depth-dependent spatial-density calculations

In Ref. 4, spatial-density calculations using the Lindhard potential are presented for $\psi_0 = 0.0°$ and $0.16°$ for several depths in the case of 1-MeV He incident near the (110) planes of Si (in this case $\epsilon = 0.0153$ and $D = 11.3$). These calculations were based on Eq. (2.35) as briefly discussed in the paragraph following the equation. For comparison, the spatial density has been calculated for $\psi_0 = 0.0°$ by using the tangent-squared potential as

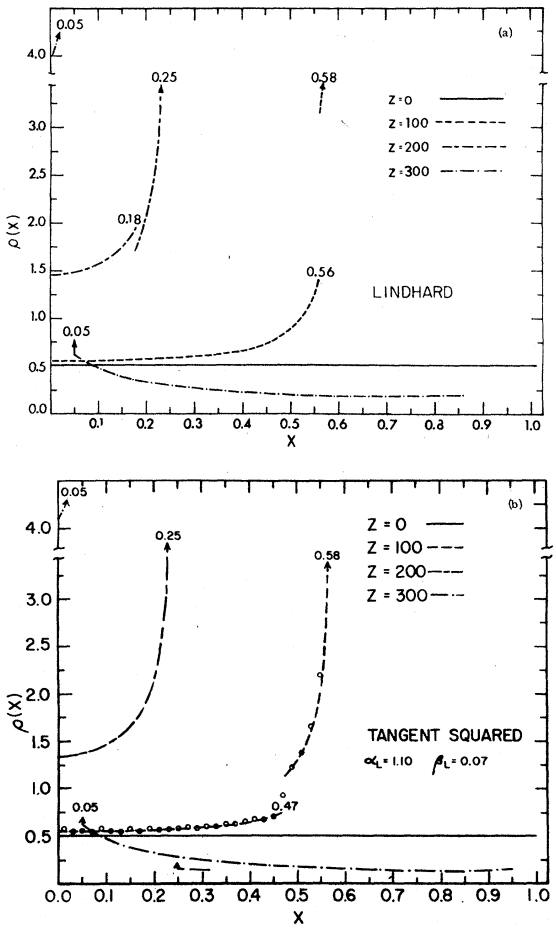

FIG. 6. Continuum-model spatial density at normalized depths of 0, 100, 200, and 300 for a perfectly aligned 1-MeV beam of He ions, uniformly distributed initially, channeled along the (110) planes of Si. Position of the jump discontinuities and infinities are marked and the density is given only for $X \geq 0$ since it is symmetric about the origin: (a) Lindhard potential is used. (b) Tangent-squared potential with $\alpha = 1.10$ and $\beta = 0.07$ is used. The open symbols in (b) for $Z = 100$ are the result of the particle-trajectory approximation discussed in Sec. IV B.

discussed in the paragraph containing Eq. (3.9), with $\epsilon = 0.0153$ and $(\alpha, \beta)_L = (1.10, 0.07)$ as determined in Sec. III B. As discussed in Sec. III A, the tangent-squared calculation is both simpler and easier to make more accurate than the corresponding calculation using the Lindhard potential.

The results of calculations for both potentials are presented in Figs. 6 and 7 for $\psi_0 = 0.0°$ and normalized depths[16] $Z = 0, 100, 200, 300, 400, 500$, and 600. The depth, in absolute units, is determined by multiplying Z by $\frac{1}{2}d_p = 0.96$ Å, as can be seen from the normalization in Sec. II A. The overall agreement is quite good. The positions of the infinities are the same with the exception of $Z = 400$. In Fig. 5, it is seen that the Lindhard and the tangent-squared wavelength functions are in excellent agreement except for those ions which start near the planes. It is these particles which cause the infinity for $Z = 400$ (see Ref. 4), hence the different values for the position of the infinity. Since the position of the jump discontinuity is determined by those particles starting nearest the planes,[4] the position of the jump discontinuities differ considerably for the two potentials.

The depth-dependent spatial density using the Moliere potential can, of course, also be calculated.

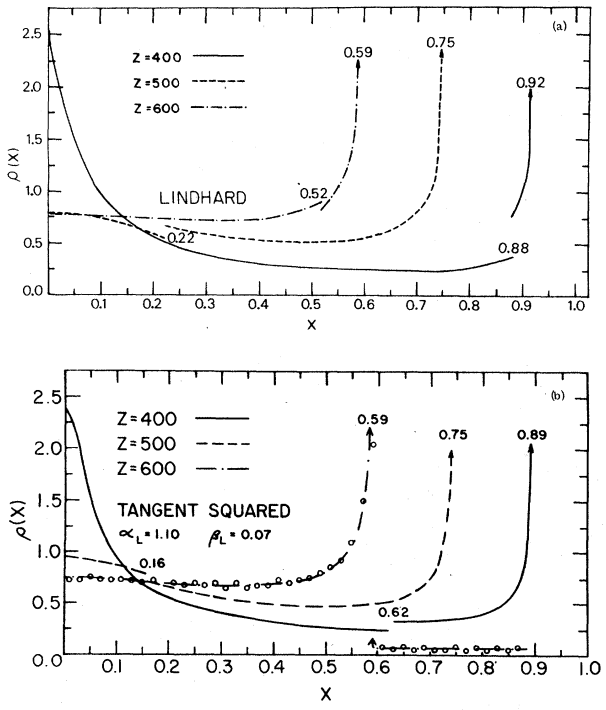

FIG. 7. As in Fig. 6 for normalized depths of 400, 500, and 600. The open sumbols in (b) for $Z = 600$ are the result of the particle-trajectory approximation discussed in Sec. IV B.

This density will differ significantly from the Lindhard calculation relative to the above results using the tangent-squared approximation. Hence, based on the current knowledge of atomic potentials, it appears reasonable to use the simpler tangent-squared potential with the two parameters, α and β, chosen by some procedure motivated by the particular situation.

B. Particle trajectory approximation to the densities

The axial-channeling spatial and momentum depth-dependent densities have been developed in a manner similar to that in Sec. II C, and, as expected, these densities are technically more difficult to compute than the planar densities. Approximations have been developed and used to compute the axial depth-dependent densities and these calculations are in good agreement with data obtained from transmission experiments in thin crystals.[17] However, since exact calculations do not exist, the accuracy of the approximations is difficult to assess. One of these approximations, the particle trajectory approximation (PTA), is easy to use in the planar-channeling case and particularly easy if the tangent-squared potential is used. In this section, we show that the PTA accurately approximates the densities of Eqs. (2.34) and (2.35). This gives added confidence in the application of this approximation to the axial case.

The PTA is based on the observation that an approximation to the depth-dependent densities ρ_Ψ and ρ_X of Eqs. (2.34) and (2.35) can be determined by numerically computing the solution of Eq. (2.7) for a large number of initial positions that are uniformly distributed over the initial interval $[-1, 1]$. The momentum density, for example, can then be approximated by noting that $\rho_\Psi(Z, \Psi)\Delta\Psi$ is approximately equal to the number of ions in $\Delta\Psi$ at depth Z, divided by the total number of ions. This approach has been used to compute an approximation to the momentum density in an *axial* channeling case[17] and a similar approach has been used in a planar case[18]; in both cases, there is good agreement with data obtained from transmission experiments in thin crystals.

We have used the tangent-squared potential with $\alpha = 0.86$, $\beta = 0.15$, and $\epsilon = 0.0153$ to compute the *momentum* density using Eq. (2.34) and to compute an approximation to this density using the PTA for $\psi_0 = 0.0°$ at a normalized depth of $Z = 600$. To compute the PTA to the density, one simply calculates $\varphi_{T_2}(600, X, 0)$ from Eq. (3.8b) for a large number of X values uniformly distributed on $[-1, 1]$, and then counts the number of function values in a given $\Delta\Psi$ interval. Again the parameters α, β, and ϵ correspond to the case of 1-MeV He incident near the

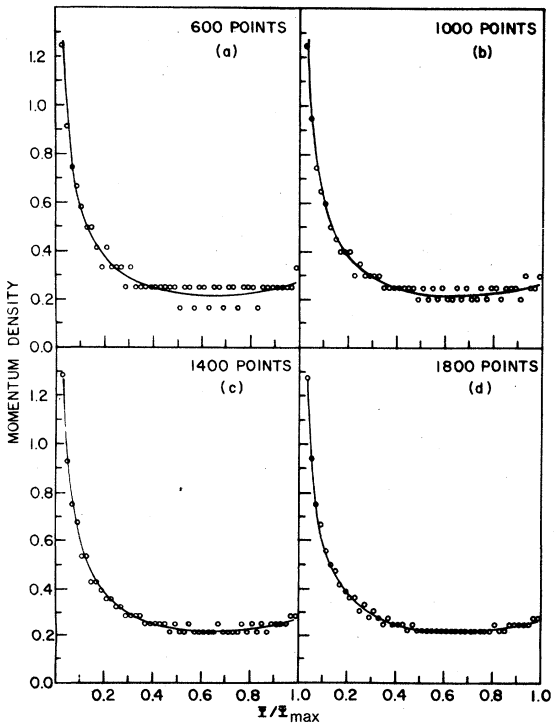

FIG. 8. Continuum-model momentum density at a normalized depth $Z=600$ for a perfectly aligned 1-MeV beam of He ions, uniformly distributed initially, channeled along the (110) planes of Si. The solid line is the result of the exact calculation using the tangent-squared approximation to the Moliere potential and the open symbols are the result of the particle-trajectory approximation: (a) 600 particles, (b) 1000 particles, (c) 1400 particles, (d) 1800 particles.

(110) planes of Si with α and β as determined in Sec. III B for the tangent-squared approximation to the Moliere potential. In Figs. 8(a)–8(d), we show the results of this calculation for the cases of 600, 1000, 1400, and 1800 particles uniformly distributed initially over the spatial interval $[-1,1]$. The open symbols are the PTA and the solid line is the actual density. For convenience, the abscissa has been taken as $\Psi/\Psi_{\max}$ where $\Psi_{\max}$ is the maximum possible Ψ for a channeled particle, in this case $\Psi_{\max}^2=\beta\tan^2\alpha=0.20$. Because of symmetry the density is presented only for $\Psi\geq 0$. The momentum density has been appropriately normalized so that its integral in the new variable, $\Psi/\Psi_{\max}$, is unity. The PTA is sensitive to the "box size" $\Delta\Psi$ and for the results shown in Fig. 8 we used $\Delta\Psi/\Psi_{\max}=0.02$.

The exact calculation shows that the momentum density has the value of 15.57 for $\Psi=0.0$, becomes infinite at $\Psi/\Psi_{\max}=0.007$, and drops to zero at $\Psi/\Psi_{\max}$, just slightly less than 1.0 (only the latter is shown on the figure). The approximation to the density for 1800 particles as shown in Fig. 8(d) is excellent; however, even the case for only 600 particles [Fig. 8(a)] shows the correct overall behavior. A characteristic feature of the approximation is that it oscillates about the true density with the oscillations becoming smaller as the number of particles increases. The magnitude of the oscillation in the interval [0.4, 0.9] in each case is due to a difference of one particle per box. In one view, the oscillations are there because the particle trajectory approximation only allows discrete values for the density, hence if the approximation overestimates the density at some value then it compensates by underestimating at a nearby value.

The PTA to the *spatial* density can also be computed. We have done this for the situation discussed in Sec. IV A, where $\alpha=1.10$, $\beta=0.07$, and $\epsilon=0.0153$, and the results are shown by the open symbols in Fig. 6(b) for $Z=100$ and in Fig. 7(b) for $Z=600$. In each case, 2000 particles have been used and the "box size" $\Delta X=0.02$ and in each case the agreement is excellent. For $Z=100$, the approximation appears to take the average value at the jump discontinuity ($X=0.47$) in the density, and for $Z=600$ it takes a value near the position of the infinity representative of the area under the infinity.

We have shown that the particle-trajectory approach can lead to excellent approximations to either the spatial or momentum density. This gives us added confidence in the axial calculations to be presented in Ref. 17. A further question of interest is how the approximation depends on depth Z, the number of particles considered, and the "box size". Apparently, the tangent-squared potential gives the simplest context in which to answer this question. It is not, however, our purpose to pursue this here.

C. Deduction of continuum potentials from planar-channeling data

Gibson and Golovchenko[7] have measured the channeled-particle wavelength as a function of transverse energy in the case of 1.8-MeV He incident along the (111) planes of Au and used the relationships in Eqs. (2.16) and (2.18) to determine an approximate continuum potential from the measured data. They used the potential-wavelength pair in absolute coordinates

$$V(x)=\tfrac{1}{2}a_1x^2+\tfrac{1}{4}a_2x^4\,, \tag{4.1}$$

$$\lambda(E_\perp)=\lambda_0(2/\pi)(1+4a_2E_\perp/a_1^2)^{-1/4}\times\mathcal{K}(\tfrac{1}{2}-\tfrac{1}{2}(1+4a_2E_\perp/a_1^2)^{-1/2})\,, \tag{4.2}$$

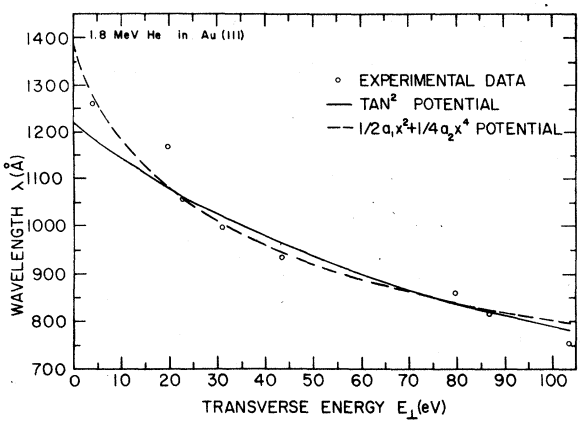

FIG. 9. Wavelength vs transverse energy for 1.8-MeV He in (111) Au channels. The open symbols are the experimental data, the dashed line is the fit to the data by Gibson and Golovchenko (Ref. 7) and the solid line is the fit to the data using the tangent-squared wavelength function.

where $\lambda_0 = \lambda(0) = 2\pi(2E/a_1)^{1/2}$ and $\mathcal{K}(m)$ is the complete elliptic integral of the first kind, with argument the parameter m. Equation (4.2) and the parameters λ_0 and a_2/a_1^2 (or equivalently a_1 and a_2) were then used to find a fit to the data; they[7] found a good fit for $\lambda_0 = 1408$ Å and $a_2/a_1^2 = 0.035$. The experimental data and the fitting function are shown in Fig. 9 by the open symbols and dashed line, respectively. The data points in the interval $20 \leq E_\perp \leq 80$ are considered to be the most reliable.

The process of finding a good fit to the data when the tangent-squared potential is used is particularly simple because of the form of Eq. (3.4). Using this equation, the reciprocal of the wavelength squared can be written as a linear function of $E_\perp$,

$$\lambda^{-2}(E_\perp) = nE_\perp + b \ , \tag{4.3}$$

where

$$n = \alpha^2/\pi^2 d_p^2 E \text{ and } b = \beta K n \ . \tag{4.4}$$

The quantities E, K, and d_p are defined in Sec. II A and α, β are the parameters of the tangent-squared potential defined in Eq. (3.1). The data points can now be fitted with a straight line to determine n and b.

Using the fact that the most reliable data points are for $20 \leq E_\perp \leq 80$, we found a good straight-line approximation to the data with $n = 9.39 \times 10^{-9}$ Å^{-2} eV^{-1} and $b = 6.69 \times 10^{-7}$ Å^{-2}. The wavelength function for these parameters is shown by the solid line in Fig. 9.

The wavelength function of Eq. (4.2) gives slightly better agreement in the region where the data is most reliable; however, both wavelength functions appear to be within the experimental error. In order to choose between the two, more accurate information is needed for small transverse energies.

Because of the linear nature of Eq. (2.18), one could superpose wavelength functions of the form of Eq. (3.4), giving more flexibility in fitting the data. The parameters would be more difficult to determine but still simpler than, say, adding the x^6 term in Eq. (4.1). The potential would no longer have a simple analytical form but it would be easy to determine from its inverse which would be a sum of arctangents [see Eq. (3.2)].

V. CONCLUSION

The elements of continuum-model planar-channeling with an emphasis on the phase-space density, which is the joint spatial-momentum density, have been discussed. This density contains all the information concerning the motion of channeled particles and its evolution is governed by the Liouville equation, which can be derived using particle conservation in the phase plane. The Liouville equation has been solved for a general initial condition by the method of characteristics giving a simple representation for the depth-dependent phase-space density as shown in Eq. (2.26). The statistical equilibrium phase-space density is easily obtained from the depth-dependent phase-space density, as was shown in Sec. II E. Thus, Eq. (2.26) allowed a unified treatment of the depth-dependent and statistical equilibrium, spatial and momentum densities for an arbitrary initial density, since all of these densities are obtained by integration from the depth-dependent phase-space density. Special attention was given to the initial density corresponding to the physically interesting case of a Gaussian-beam divergence. This led to new representations for the associated densities [see Eqs. (2.39), (2.50) and discussion following Eq. (2.50)] which would be easier to use than equivalent representations obtained by convoluting the zero beam divergence densities with a Gaussian.

A new planar-continuum potential, the tangent-squared potential, has been introduced and it is shown that the wavelength function and the solutions of the equations of motion can be written in terms of elementary functions. This gives an elementary expression for the phase-space density of Eq. (2.26). After comparing this potential with the Lindhard and the Moliere potentials, and after using it to analyze some experimental data of Gibson and Golovchenko,[7] we conclude that it is a physically reasonable potential. We also demonstrated that in certain calculations it is much easier to use than the potentials of either Lindhard or

Moliere. In fact, for computations which can make use of the wavelength function or the solutions of the equations of motion, it is easier to use than either the hyperbolic cosine potential or the simple anharmonic potential ($\frac{1}{2}a_1x^2+\frac{1}{4}a_2x^4$), both of which were introduced to simplify channeling calculations. This is because the wavelength function and the solutions of the equation of motion for the latter two potentials require the use of the more complex complete elliptic integrals and Jacobi elliptic functions. Finally, we have shown that the particle-trajectory approximation, which is quite useful in the axial case,[17] gives excellent agreement with the exact calculation in the planar case.

Since useful perturbation schemes rely on being able to find, in some reasonable form, the zeroth order approximation, we are investigating the possibility of studying thermal vibrations and electron multiple scattering by a perturbation analysis based on the Liouville equation and the tangent-squared potential.

ACKNOWLEDGMENTS

The major portion of this work was completed during a sabbatical leave spent with the Physics Department at the State University of New York in Albany. I appreciated the congenial atmosphere they created and I gratefully acknowledge their support. My thanks to D. K. Brice, S. T. Chui, W. M. Gibson and S. T. Picraux for many enjoyable and helpful discussions concerning the nature and applications of channeling.

---

*Present address: Dept. of Mathematics, University of New Mexico, Albuquerque, N. M. 87131.

[1](a) *Channeling: Theory, Observation and Applications*, edited by D. V. Morgan (Wiley, New York, 1973); (b) D. S. Gemmell, Rev. Mod. Phys. 46, 129 (1973).

[2]S. Datz, C. D. Moak, T. S. Noggle, B. R. Appleton, and H. D. Lutz, Phys. Rev. 179, 315 (1969); and M. T. Robinson, *ibid.* 179, 327 (1969).

[3]F. Abel, G. Amsel, M. Bruneaux, C. Cohen, and A. L'Hoir, Phys. Rev. B 13, 993 (1976).

[4]J. A. Ellison, Phys. Rev. B 12, 4771 (1975).

[5]L. D. Landau and E. M. Lifshitz, *Mechanics* (Addison-Wesley, Reading, Mass., 1969).

[6]J. A. Ellison and S. T. Picraux, (a) Sandia Laboratories Report No. SAND 77-0361 (unpublished, 1977); and (b) Phys. Rev. B 18, 1028 (1978).

[7]W. M. Gibson and J. Golovchenko, Phys. Rev. Lett. 28, 1301 (1972).

[8]K. Huang, *Statistical Mechanics* (Wiley, New York, 1963).

[9]M. A. Kumakhov, Radiat. Eff. 26, 43 (1975).

[10]M. A. Kumakhov and R. Wedell, Radiat. Eff. 30, 1 (1976).

[11]This equation can be derived directly by probabilistic methods. In fact, the entire development of the spatial, momentum, and phase-space densities, in Secs. II C–II E could proceed from the equations $X(Z)=\varphi_1(Z,X_i,\Psi_i)$ and $\Psi(Z)=\varphi_1(Z,X_i,\Psi_i)$, where φ_1 and φ_2 are defined in Eq. (2.24). Here, X_i and Ψ_i are to be considered random variables defined by their joint density σ_0, and $X(Z)$ and $\Psi(Z)$ are depth-dependent functions of these random variables. The various densities associated with $X(Z)$ and $\Psi(Z)$ are determined by the standard methods for finding densities of nonlinear functions of random variables. A discussion of this approach is contained in T. L. Saaty, *Modern Nonlinear Equations* (McGraw-Hill, New York, 1967), p. 350 ff.

[12]The identity $\delta(f(x))=\delta(x-x_0)/|f'(x_0)|$ where $f(x_0)=0$ has been used.

[13]J. A. Ellison and T. Guinn, Phys. Rev. B 13, 1880 (1976).

[14]These solutions can be derived by solving the first-order ordinary differential equation associated with the energy equation, Eq. (2.9), using the fact that an indefinite integral of $[(1+E)/(E-\tan^2 x)]^{1/2}$ is $\sin^{-1}\{[(1+E)/E]^{1/2}\sin x\}$.

[15]Abel *et al.* in Ref. 3 have apparently used this approach to compute the spatial density for $\Psi_0=0.0$ after finding an analytic approximation to the function $\varphi_1(Z,X,0)$ as determined by the Lindhard potential.

[16]In Ref. 4, it is incorrectly stated that the depth is in angstroms. The mistake in the paper is corrected if s_0, as defined in Eq. (4) of that paper, is taken to be $\frac{1}{2}d_p$ [which is 0.96 Å for (110) Si] rather than 1 Å as stated on p. 4773. Hence, Fig. 2 of that paper is corrected by multiplying the ordinate by 0.96 and Figs. 6–11 are corrected by multiplying the values of the abscissa by 0.96. For example, in Fig. 8 [which corresponds to Fig. 7a of this paper], the curves given are for depths of 384, 480, and 576 Å rather than 400, 500, and 600 Å as stated.

[17]J. A. Ellison, S. T. Chui, and W. M. Gibson, Phys. Rev. B (to be published).

[18]H. O. Lutz, R. Ambros, C. Mayer-Boricke, J. Reichelt, and M. Rogge, Z. Naturforsch. A 26, 1105 (1971).